Speciating volatile organic compounds in indoor air: using in-situ GC to interpret real-time PTR-MS signals

Jenna C. Ditto[1,*], Han N. Huynh[2,3], Jie Yu[4], Michael F. Link[5], Dustin Poppendieck[5], Megan S. Claflin[6], Marina E. Vance[7], Delphine K. Farmer[8], Arthur W.H. Chan[4,9], Jonathan P.D. Abbatt[4]

[1]Department of Energy, Environmental, and Chemical Engineering, Washington University in St. Louis; [2]Cooperative Institute for Research in Environmental Sciences (CIRES), University of Colorado Boulder; [3]NOAA Chemical Sciences Laboratory; [4]Department of Chemistry, University of Toronto; [5] Engineering Laboratory, National Institute of Standards and Technology; [6]Aerodyne Research, Inc.; [7]Department of Mechanical Engineering, University of Colorado Boulder; [8]Department of Chemistry, Colorado State University; [9]Department of Chemical Engineering and Applied Chemistry, University of Toronto

*Correspondence: dittoj@wustl.edu

Number of pages: 32
Number of tables: 7
Number of figures: 28

Section S1. Descriptions of additional target chemicals

a. Example compounds with dominant peak as parent ion (> 75 % of EIC)

Ethanol: Ethanol was the sole peak in the EIC at $C_2H_6OH^+$, and this contribution remained consistent throughout the different indoor experiments and outdoor samples during the campaign. Overall, this is consistent with Coggon et al.'s observations from GC-PTR-MS in urban outdoor air that ethanol measured at its proton transfer adduct did not have major other contributing peaks in its chromatogram (1). Some key sources of ethanol indoors include human breath, cleaning products, and food products/cooking (2). As mentioned in the main text, due to the relatively high role of the baseline signal relative to ethanol's signal in the EIC, the EIC was not integrated here and 100% of the signal was attributed to ethanol.

D4 siloxane: D4 siloxane was the sole peak in the EIC at $C_8H_{24}O_4Si_4H^+$. Indoors, key sources of D4 siloxane include personal care products and adhesives (3). As mentioned in the main text, due to the relatively high role of the baseline signal relative to D4 siloxane's signal in the EIC, the EIC was not integrated here and 100% of the signal was attributed to D4 siloxane.

D5 siloxane: D5 siloxane was the sole peak in the EIC at $C_{10}H_{30}O_5Si_5H^+$. The most important source of D5 siloxane in the indoor environment is personal care product use (3). As mentioned in the main text, due to the relatively high role of the baseline signal relative to D5 siloxane's signal in the EIC, the EIC was not integrated here and 100% of the signal was attributed to D5 siloxane.

Acetonitrile: On average, acetonitrile contributed 79 ± 6 % to the EIC at $C_2H_3NH^+$. Other contributing peaks in the EIC were consistently limited indoors, but increased during outdoor sampling mostly due to low outdoor signal of acetonitrile and lower signal-to-noise ratios that may have caused an apparent increase in non-acetonitrile signal at this EIC. Both

acetonitrile and acrylonitrile peaks had a slight shoulder, which could have contributed to an apparent interference at both EICs. Indoors, acetonitrile may arise from cooking (4,5), and along with acrylonitrile (discussed more below), from wood combustion (6,7).

b. Example compounds with significant contributions from peaks eluting within of 100 sec from the parent ion's retention time (> 25 % of EIC)

1,4-Dioxane: The levels of confounding EIC peaks for 1,4-dioxane were significant, and 1,4-dioxane itself contributed on average 8 ± 3 % of its EIC indoors. EICs indoors and outdoors were similar but complex and consisted mostly of closely eluting peaks, which could include isomers, and with some important contributions from peaks outside of the 100 sec window as well, which could include fragments and unknown ions. Isomers could include other dioxane structures as well as acids (e.g., butyric acid, isobutyric acid), ethyl acetate, hydroxybutanals, and others. 1,4-dioxane is not commonly measured in indoor air, but it may exist as a trace contaminant in some personal care and consumer products.

2-Heptanone: 2-Heptanone contributed on average 49 ± 6 % of the EIC at $C_7H_{14}OH^+$, once again with fairly consistent contributions from other species in its EIC across indoor experiments. Like the 6-carbon carbonyls, these other species were almost exclusively closely eluting carbonyl isomers (3-heptanone, 2-heptanone, and heptanal). Indoors, 2-heptanone may arise from wood products (8).

c. Example compounds with higher sensitivity to indoor conditions

Toluene: Toluene contributed on average 55 ± 12 % to the EIC at $C_7H_9^+$. The contributions of non-toluene peaks were smaller for smoke experiments and for outdoor samples. As with benzene, fragmentation products contributed significantly to interferences at this EIC including from trimethylbenzenes, ethyl toluenes, and some monoterpenes (α-pinene, in our

case). We observed much more interference in this indoor environment and with these instrument operating conditions relative to Coggon et al., who observed 95 % of the m/z 93 signal in Las Vegas to be toluene with a small contributing peak of 1-ethyl-3-methylbenzene.(1) This emphasizes the need for robust analyses of contributions from isobaric species, fragmentation products interferences, and the role of unknown peaks sampled in a range of indoor environments with PTR-MS, as outdoor observations may not always be applicable in the indoor environment.

Acrylonitrile: Acrylonitrile contributed on average 70 ± 14 % of its indoor EIC at $C_3H_3NH^+$. Contributions of fragments and unknown ions were very limited indoors. Outdoors, we observed occasional contribution from two low abundance, unidentified peaks. Indoors, the largest non-acrylonitrile contribution came from a low abundance closely eluting peak or peak shoulder.

Section S2. Considering the role of ozone in forming positive and negative artifacts

The presence of ozone indoors and its possible role in the formation of positive and negative sampling artifacts (especially for instruments operated without an ozone scrubber, which was the case here (9)) is important to consider. Ozone mixing ratios in the house ranged from 0 ppb to 37 ppb during GC-PTR-MS measurements, but outside of specific ozone addition experiments, mixing ratios were maintained below 10 ppb during GC sampling (Table S1). Ozone can react with adsorbent materials (e.g., Tenax TA) to form some short-chain C_6-C_{10} aldehyde positive artifacts (e.g., as observed with 100 ppb O_3 by Lee et al. (10)). It can also deplete ozone-reactive species, like terpenes, while they are trapped on the adsorbent material prior to chromatography. This may yield negative artifacts.

To reduce the possible impact of positive artifact aldehydes formed from ozone-Tenax TA reactions in the adsorbent trap, we integrated all peaks in zero air samples and subtracted the nearest collected zero air sample from all indoor ambient samples. Contributions of aldehyde peaks to zero air samples did not increase throughout the campaign, which would have been expected if significant ozonolysis artifacts formed throughout the periodic ozone experiments and persisted in the thermal desorption system. For instance, a comparison of zero air peaks is shown for nonanal in Figure S2; nonanal is chosen here as it is a known positive artifact, and no upward trend in signal with time is observed.

We also compared the instrument sensitivity as calculated from real time PTR-MS measurements (without any adsorbent material susceptible to ozonolysis artifacts in the flow path) and from GC-PTR-MS measurements and found good agreement for calibrated species. Figure S3 shows an illustrative time series of hexanal, which *could* be a positive ozone-related artifact, but has good agreement between GC and real time PTR signals. If hexanal were formed in large amounts as a positive artifact, we would expect the signal in GC samples to be higher relative to real-time PTR samples. Similarly, Figure S4 shows a comparison of all field- and lab-calibrated species from the calibration gases mentioned above. Here too, there is generally good agreement between both measurement types.

Focusing on the agreement between ozone-reactive terpenes, which could have been depleted by ozone reactions while these terpenes were trapped on the adsorbent material to yield negative artifacts, we see that they are biased slightly low in GC vs. real time PTR measurements but that they follow the same trend as other non-ozone-reactive species.

Taken together, we conclude that we did not observe significant influence of positive or negative artifacts here, but discuss them briefly here to emphasize them as important factors to consider that could impact GC-PTR-MS results indoors.

Section S3. Relative consistency in isomer contributions

Many of the above species had several likely isomer structures present in their EICs, but here we select a subset of compounds with clear isomer patterns that could be readily tracked across all chromatograms collected during the campaign (Figure S28).

We expect the contribution of aldehydes to the total tracked carbonyls to increase in certain experiments, namely cooking and ozonolysis experiments as described above. During cooking, both hexanal and octanal showed greater contributions relative to their isomers, rising towards the upper end of the range of aldehyde contributions across the full experiment set; hexanal's relative contribution to the C6 carbonyls during cooking was 87 % (contributions of hexanal to the C6 carbonyl set across all indoor experiments ranged from 77 % to 90 %) while octanal's relative contribution to the C8 carbonyls during cooking was 85 % (range: 69 % to 86%). The relative contribution of pentanal and heptanal were not enriched during cooking (pentanal's relative contribution was 35 % (range: 20 % to 67 %), while heptanal's relative contribution was 22 % (range: 19 % to 35 %)). However, all of these aldehydes showed absolute signal enhancements during cooking, while their relative contributions remained consistent.

During experiments involving ozone, either ozone injections to the house or experiments involving aged smoke (which was mixed with ozone and allowed to chemically react before injection to the house), aldehyde contributions tended to be slightly higher relative to other carbonyls. For pentanal, contributions during ozone experiments ranged from 61 % to 67 %

(overall range of pentanal contributions to the C5 carbonyl signal: 20 % to 67 %). For hexanal, this ranged from 83 % to 88 % (overall range: 77 % to 90 %). For heptanal, this ranged from 32 % to 34 % (overall range: 19 % to 35 %). For octanal, this ranged from 83 % to 86 % (overall range: 69 % to 86 %). As we noted above, while ozone mixing ratios during GC sampling were low in the house, the relationship with ozone is still complex; these aldehydes could be ozonolysis products of higher molecular weight unsaturated organic compounds or positive artifacts due to ozone reactions in inlet tubing and/or in the thermal desorption unit. Given the investigations into possible positive artifact formation described in Section S2, it is more likely in this case that these aldehydes are ozonolysis products from chemistry occurring in the house.

The relative contributions of the three trimethylbenzenes and xylenes were consistent throughout the campaign (for example, 1,3,5-trimethylbenzene ranged only from 12 % to 15 % of the $C_9H_{13}^+$ EIC for all sources and chemical conditions).

Similar to the aldehyde discussion above, we expect the monoterpene distribution to be most sensitive to emission source and ozone mixing ratio. These tentative monoterpene identifications were based on retention indices from authentic standards run with the system at the end of the campaign. Due to the lack of humans living in the house and thus limited number of fragranced products applied, the monoterpene distribution reflected infiltration and building material emissions more strongly. The monoterpene distribution was dominated by α-pinene, the first peak in the series (outdoors α-pinene contributed 60 % of the monoterpene signal, while indoors it ranged tightly from 53 % to 60 %). In addition to infiltrated α-pinene, most of the observed α-pinene likely arose from the building itself (given that indoor concentrations were 2 orders of magnitude higher than outdoor concentrations, Figure S16). This is consistent with observations in the NZERTF following initial construction, where Poppendieck et al. measured

α-pinene emission rates at 9-11 times limonene's emission rates. The second monoterpene peak, proposed to be camphene based on its Kovats retention index, showed little source or chemical condition sensitivity (relative contributions ranged from 2 % to 5 %). The third peak, proposed to be β-pinene, showed greater variability and also greater contributions during aged smoke experiments (contributions ranged from 16 % to 27 %). The fourth peak, proposed to be carene, ranged from 10 % to 14% and did not show much source or chemical condition sensitivity. Limonene, the final peak in the series, ranged from 4 % to 12% contribution to the monoterpene signal. Overall, in this environment, the monoterpene distribution remained relatively stable, but reflects building material emissions more strongly than consumer product emissions (i.e., signal enriched in α-pinene rather than limonene). While this may not be true in every indoor environment, it is an important feature of the unoccupied home studied here. This is another illustration of the benefit to incorporating isomer speciation; without upstream GC measurements, it would not be possible to know which terpenes contributed the most to the overall $C_{10}H_{17}^+$ signal, and thus it would not be possible to accurately assess properties like ozone reactivity of the mixture.

Table S1. Summary of experiments captured by GC-PTR-MS sampling. ACR refers to air change rate.

First sample start and last sample stop of GC sequence (local time)	Nearest experiment captured by GC-PTR-MS	Average environmental conditions during sampling	Key experiment details
Start: 3/15/22 17:20:36 Stop: 3/15/22 18:10:51	Cooking (sampled during experiment)	T=24.0 °C RH=30.3 % O_3=29.3 ppb ACR=0.2 h^{-1}	Sequential pan frying of peppers (104 g, 300 F max temperature), tater tots (201 g, 200 F max temperature), and bacon (109 g, 240 F), in 10 g canola oil
Start: 3/17/22 1:00:38 Stop: 3/17/22 2:10:57	Acid-base, cooking (sampled early the next morning immediately following experiment)	T=23.3 °C RH=54.2 % O_3=8.3 ppb ACR=0.2 h^{-1}	Combined pan frying of 122 g onions, 113 g peppers, 138 g zucchini, 105 g mushrooms to max temperature of 210 F with a balsamic glaze Test NH_3 injections of 300 mL/min, 600 mL/min, 1200 mL/min of 10 % NH_3 diluted in N_2
Start: 3/18/22 3:35:14 Stop: 3/18/22 4:45:33	Acid-base (sampled early the next morning immediately following experiment)	T=24.9 °C RH=47.8 % O_3=0 ppb ACR=0.2 h^{-1}	Repeated NH_3 and CO_2 injections for 30 minutes each, 40 mg/min NH_3 and 500 g/min CO_2, spaced out every 3 hours
Start: 3/20/22 2:39:04 Stop: 3/20/22 23:29:18	Background (sampled during experiment)	T=24.9 °C RH=32.7 % O_3=7.1 ppb ACR=0.2 h^{-1}	No house activities
Start: 3/23/22 3:16:09 Stop: 3/23/22 4:26:26	Fresh smoke + ozone (sampled early the next morning immediately following experiment)	T=24.0 °C RH=27.0 % O_3=7.4 ppb ACR=0.2 h^{-1}	Repeated test injections of wood smoke followed by test ozone injections to the house
Start: 3/25/22 8:20:26 Stop: 3/25/22 16:47:35	Fresh smoke (sampled during experiment)	T=24.0 °C RH=30.1 % O_3=7.2 ppb ACR=0.2 h^{-1}	0.35-0.5 g woodchips burned over four separate instances spaced out by 2.5 hours, various air cleaning technologies implemented 45 mins after each of the first three burns

First sample start and last sample stop of GC sequence (local time)	Nearest experiment captured by GC-PTR-MS	Average environmental conditions during sampling	Key experiment details
Start: 3/27/22 0:11:54 Stop: 3/27/22 17:51:10	Background (sampled during experiment)	T=23.8 °C RH=22.0 % O_3=6.1 ppb ACR=0.2 h^{-1}	No house activities until 18:00, then humidification began at 18:00
Start: 3/27/22 18:01:13 Stop: 3/27/22 23:52:55	Background + RH (sampled during experiment)	T=23.9 °C RH=52.1 % O_3=7.5 ppb ACR=0.2 h^{-1}	
Start: 3/28/22 20:34:22 Stop: 3/28/22 22:44:45	Outdoor	House not measured	Outdoor
Start: 3/29/22 6:25:50 Stop: 3/29/22 8:16:22	Background + RH (measured during background period before the day's experiments)	T=25.7 °C RH=73.4 % O_3=6.2 ppb ACR=0.2 h^{-1}	Background + RH at the start of the day, then captured fresh smoke addition from 0.51 g woodchips
Start: 3/29/22 9:06:48 Stop: 3/29/22 9:57:02	Fresh smoke + RH (measured during experiment)	T=25.9 °C RH=73.9 % O_3=6.1 ppb ACR=0.2 h^{-1}	
Start: 3/30/22 7:09:17 Stop: 3/30/22 9:43:37	Background + RH (measured during background before the experiments)	T=25.8 °C RH=73.7 % O_3=0.7 ppb ACR =0.2 h^{-1}	Background + RH at the start, then aged smoke created from 6.37 g wood chips burned and added to a Teflon bag with 19.5 ppm ozone in bag (allowed to age together before injection to house)
Start: 3/30/22 9:55:19 Stop: 3/30/22 10:45:35	Aged smoke + RH (measured during experiment)	T=26.0 °C RH=73.5 % O_3=1.9 ppb ACR =0.2 h^{-1}	
Start: 4/3/22 0:10:09 Stop: 4/3/22 22:59:00	Outdoor	House not measured	Outdoor
Start: 4/5/22 8:31:25 Stop: 4/5/22 10:21:51	Fresh smoke (sampled during experiment)	T=23.7 °C RH=29.9 % O_3=12.5 ppb ACR =0.2 h^{-1}	0.5 g wood chip smoke added to the house, followed by a period of ozone addition for 30 mins, followed by another 0.5 g wood chip smoke addition to the house, followed by a final period of ozone addition for 30 mins
Start: 4/5/22 11:12:20 Stop: 4/5/22 17:56:54	Fresh smoke + O_3 (sampled during experiment)	T=23.7 °C RH=33.4 % O_3=31.2 ppb ACR =0.2 h^{-1}	

First sample start and last sample stop of GC sequence (local time)	Nearest experiment captured by GC-PTR-MS	Average environmental conditions during sampling	Key experiment details
Start: 4/5/22 18:06:58 Stop: 4/5/22 19:50:17	Fresh smoke (sampled during experiment)	T=23.7 °C RH=36.2 % O_3=6.1 ppb ACR=0.2 h^{-1}	
Start: 4/5/22 20:00:21 Stop: 4/6/22 0:18:06	Fresh smoke + O_3 (sampled during experiment)	T=23.7 °C RH=36.3 % O_3=36.6 ppb ACR=0.2 h^{-1}	
Start: 4/6/22 9:07:48 Stop: 4/6/22 9:16:48	Background (sampled during experiment)	T=23.6 °C RH=36.6 % O_3=8.4 ppb ACR=0.2 h^{-1}	Background sample, then captured aged smoke (made from 20 ppm ozone in bag, mixed with wood chip smoke and allowed to react prior to injecting to the house), then added ozone to the whole house, then finally prepared more aged smoke (with 21 ppm ozone in bag and wood chip smoke) and injected to house
Start: 4/6/22 9:27:51 Stop: 4/6/22 10:58:10	Aged smoke (sampled during experiment)	T=23.6 °C RH=35.9 % O_3=7.6 ppb ACR=0.2 h^{-1}	
Start: 4/6/22 11:48:33 Stop: 4/6/22 16:32:36	Aged smoke + O_3 (sampled during experiment)	T=23.7 °C RH=36.3 % O_3=30.3 ppb ACR=0.2 h^{-1}	
Start: 4/6/22 17:23:00 Stop: 4/7/22 0:50:18	Aged smoke (sampled during experiment)	T=23.7 °C RH=37.3 % O_3=7.9 ppb ACR=0.2 h^{-1}	
Start: 4/9/22 18:35:43 Stop: 4/10/22 12:36:11	No ventilation (sampled during experiment)	T=24.3 °C RH=28.6 % O_3=9.0 ppb ACR=0 h^{-1}	Mechanical ventilation reduced to 0 CFM on 4/9/22 at 18:30, all the way through sample end time on 4/10/22
Start: 4/10/22 14:03:01 Stop: 4/10/22 16:53:42 Start: 4/10/22 18:12:41 Stop: 4/10/22 23:24:02	Outdoor Background (sampled during experiment)	House not measured T=24.0 °C RH=25.2 % O_3=n/a ACR=0.2	Sampled outdoors, then switched to sampling indoors during background period after ventilation had been turned back on 4/10/22 at 16:04

Table S2. Number of samples in each category of indoor conditions.

Indoor condition	Number of samples
Background	59
Background + RH	26
No ventilation	43
Acid-base	8
Cooking	7
Smoke	26
Smoke + RH	3
Smoke + O_3	31
Aged smoke	23
Aged smoke + RH	3
Aged smoke + O_3	12
Outdoor	65

Table S3. Carbonyl summary mixture-weighted property data.

C5 Carbonyls	**Log(K_{oa})**	**H (atm×m^3/mol)**
Pure 2-Pentanone	3.38×10^{0}	7.92×10^{-5}
Pure Pentanal	3.53×10^{0}	1.69×10^{-4}
Mix mean	3.51×10^{0}	1.56×10^{-4}
Mix median	3.51×10^{0}	1.57×10^{-4}
C6 Carbonyls	**Log(K_{oa})**	**H (atm×m^3/mol)**
Pure 3-Hexanone	3.53×10^{0}	1.12×10^{-4}
Pure 2-Hexanone	3.80×10^{0}	1.12×10^{-4}
Pure Hexanal	3.84×10^{0}	2.39×10^{-4}
Mix mean	3.83×10^{0}	2.35×10^{-4}
Mix median	3.84×10^{0}	2.37×10^{-4}
C7 Carbonyls	**Log(K_{oa})**	**H (atm×m^3/mol)**
Pure 3-Heptanone	4.16×10^{0}	1.58×10^{-4}
Pure 2-Heptanone	4.14×10^{0}	1.58×10^{-4}
Pure Heptanal	4.25×10^{0}	3.38×10^{-4}
Mix mean	4.22×10^{0}	2.89×10^{-4}
Mix median	4.22×10^{0}	2.92×10^{-4}
C8 Carbonyls	**Log(K_{oa})**	**H (atm×m^3/mol)**
Pure 3-Octanone	4.50×10^{0}	2.23×10^{-4}
Pure 2-Octanone	4.48×10^{0}	2.23×10^{-4}
Pure Octanal	4.46×10^{0}	4.77×10^{-4}
Mix mean	4.46×10^{0}	4.67×10^{-4}
Mix median	4.46×10^{0}	4.69×10^{-4}

Table S4. Monoterpene summary mixture-weighted property data.

Monoterpenes	k_{O3} (cm^3/molecules×s)
Pure α-pinene	4.30×10^{-16}
Pure camphene	1.14×10^{-17}
Pure β-pinene	1.20×10^{-17}
Pure carene	4.30×10^{-16}
Pure Limonene	4.42×10^{-16}
Mix mean	3.87×10^{-16}
Mix median	3.90×10^{-16}

Table S5. Average percent contribution of parent chemical peak across indoor conditions.

Parent chemical	Background	Background + RH	No ventilation	Acid base	Cooking
Isoprene	0.4	1.9	0.5	1.7	3.5
Benzene	20.5	19.9	12.5	21.4	19.7
Toluene	32.6	49.5	40.1	57.1	43.6
o-Xylene	32.4	30.9	30.2	42.0	48.8
1,3,5-Trimethylbenzene	12.2	16.1	11.2	10.3	9.2
Alpha pinene	55.6	56.0	56.9	60.4	75.1
Limonene	7.1	7.8	8.6	8.5	10.0
Acetonitrile	77.9	84.2	80.1	71.3	76.0
Acrylonitrile	51.7	60.5	61.3	76.6	79.2
Pyrrole	94.4	89.7	89.8	98.2	97.9
Chlorobenzene	82.6	67.6	58.8	96.5	97.3
D4 Siloxane	100	100	100	100	100
D5 Siloxane	100	100	100	100	100
Ethanol	100	100	100	100	100
Acrolein	50.2	49.2	60.2	45.8	49.0
Acetone	79.9	80.5	82.7	79.0	73.8
Furan	42.1	30.5	43.9	26.3	30.2
2-Butanone	60.7	56.2	62.1	52.6	49.9
Butanal	10.7	12.2	15.6	7.1	5.3
1,4-Dioxane	7.2	9.0	10.0	5.3	4.0
Furfural	78.4	79.5	80.9	79.1	79.2
2-Hexanone	7.5	8.9	7.9	12.5	10.1
Hexanal	71.1	69.1	75.0	66.0	68.1
2-Heptanone	46.7	48.4	41.4	60.1	57.7
Nonanal	84.5	84.6	84.4	85.0	88.4

Table S6. Average percent contribution of parent chemical peak across indoor conditions.

Parent chemical	Smoke	Smoke + RH	Smoke + O_3	Aged smoke	Aged smoke + RH	Aged smoke + O_3
Isoprene	4.1	6.0	1.2	1.6	4.3	1.3
Benzene	41.3	22.3	29.9	33.6	20.7	25.3
Toluene	59.6	72.3	63.2	63.1	69.3	55.2
o-Xylene	29.5	33.3	30.3	30.5	29.0	30.0
1,3,5-Trimethylbenzene	13.2	19.6	13.1	11.7	12.0	11.0
Alpha pinene	53.1	58.4	54.7	56.0	53.6	55.7
Limonene	8.1	8.4	4.7	6.7	9.1	4.1
Acetonitrile	75.0	74.8	82.7	75.4	91.8	82.1
Acrylonitrile	68.2	45.7	75.7	86.8	73.7	86.9
Pyrrole	94.5	90.8	86.8	87.7	92.1	84.0
Chlorobenzene	83.3	66.6	61.6	71.9	35.5	69.5
D4 Siloxane	100	100	100	100	100	100
D5 Siloxane	100	100	100	100	100	100
Ethanol	100	100	100	100	100	100
Acrolein	55.4	57.9	61.4	70.7	50.1	65.6
Acetone	76.1	82.1	79.0	79.7	79.5	79.7
Furan	48.9	36.4	52.0	56.2	36.3	55.1
2-Butanone	57.5	51.9	57.7	58.6	59.5	64.5
Butanal	7.8	8.0	7.9	9.4	9.5	12.8
1,4-Dioxane	5.7	10.0	8.7	9.1	14.1	9.7
Furfural	76.7	80.7	78.3	78.3	80.4	78.8
2-Hexanone	7.9	10.1	5.7	7.4	10.7	7.7
Hexanal	70.1	68.9	72.7	72.5	67.2	73.4
2-Heptanone	49.0	50.3	43.6	43.3	53.0	42.0
Nonanal	88.1	86.0	88.5	85.6	86.2	87.5

Table S7. Average percent contribution of parent chemical peak across indoor conditions.

Parent chemical	Outdoor	Indoor average	Indoor standard deviation
Isoprene	20.1	2.4	1.8
Benzene	43.2	24.3	7.9
Toluene	72.8	55.1	12.4
o-Xylene	23.1	33.4	6.3
1,3,5-Trimethylbenzene	10.3	12.7	2.9
Alpha pinene	77.4	57.8	6.1
Limonene	6.5	7.6	1.8
Acetonitrile	54.7	79.2	5.8
Acrylonitrile	98.0	69.7	13.6
Pyrrole	70.3	91.4	4.5
Chlorobenzene	13.1	71.9	17.8
D4 Siloxane	100	100	-
D5 Siloxane	100	100	-
Ethanol	100	100	-
Acrolein	37.6	56.0	7.9
Acetone	83.4	79.3	2.5
Furan	55.3	41.6	10.5
2-Butanone	91.2	57.4	4.5
Butanal	17.4	9.7	3.0
1,4-Dioxane	4.1	8.4	2.8
Furfural	67.7	79.1	1.2
2-Hexanone	16.6	8.8	1.9
Hexanal	33.9	70.4	2.8
2-Heptanone	35.8	48.7	6.2
Nonanal	84.9	86.3	1.6

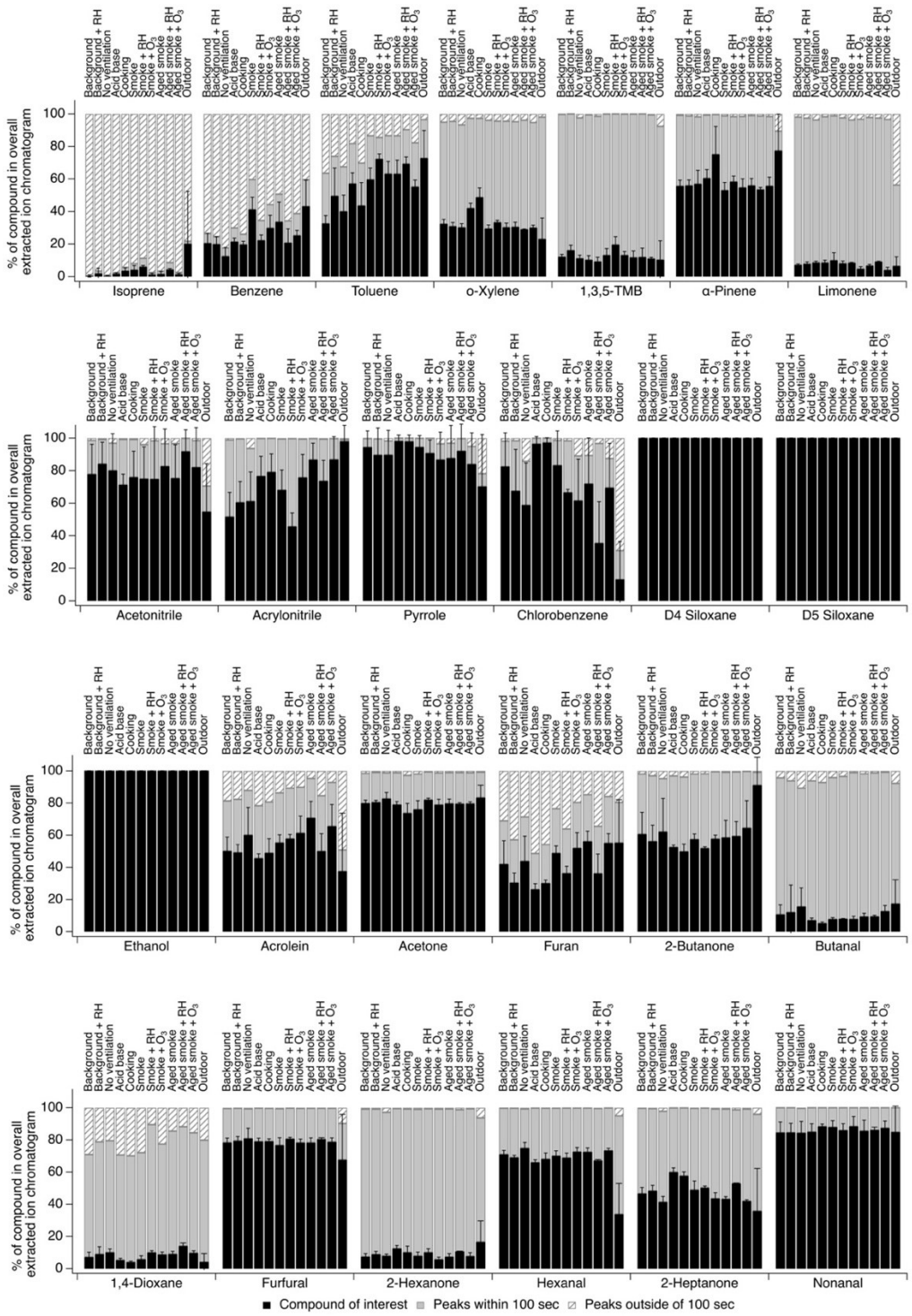

Figure S1. Mean percent contribution of compound of interest (black) to the extracted ion chromatogram for select hydrocarbon, chlorinated, and nitrogenous species. Peaks eluting within 100 sec are shown in grey, and peaks eluting outside of 100 sec are shown in crosshatched grey. Error bars represent standard deviation from the mean. Data are tabulated in Table 1 and in Tables S5-S7. Data are shown to complement main text Figures 2-4.

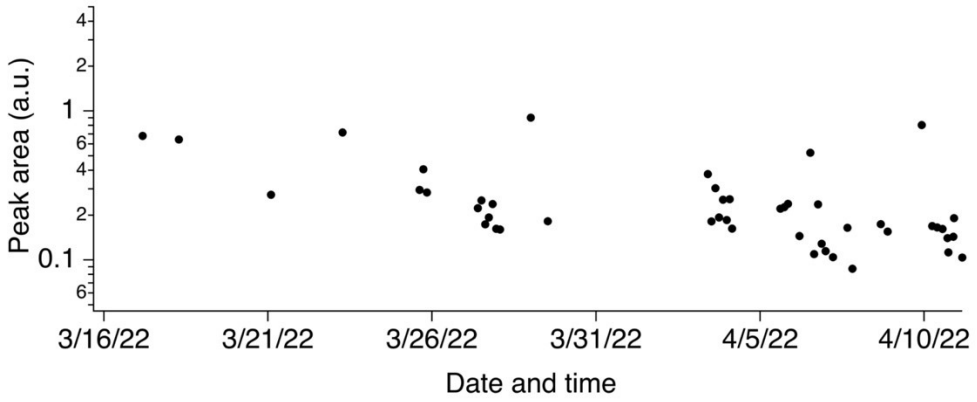

Figure S2. Nonanal peak area from zero air samples.

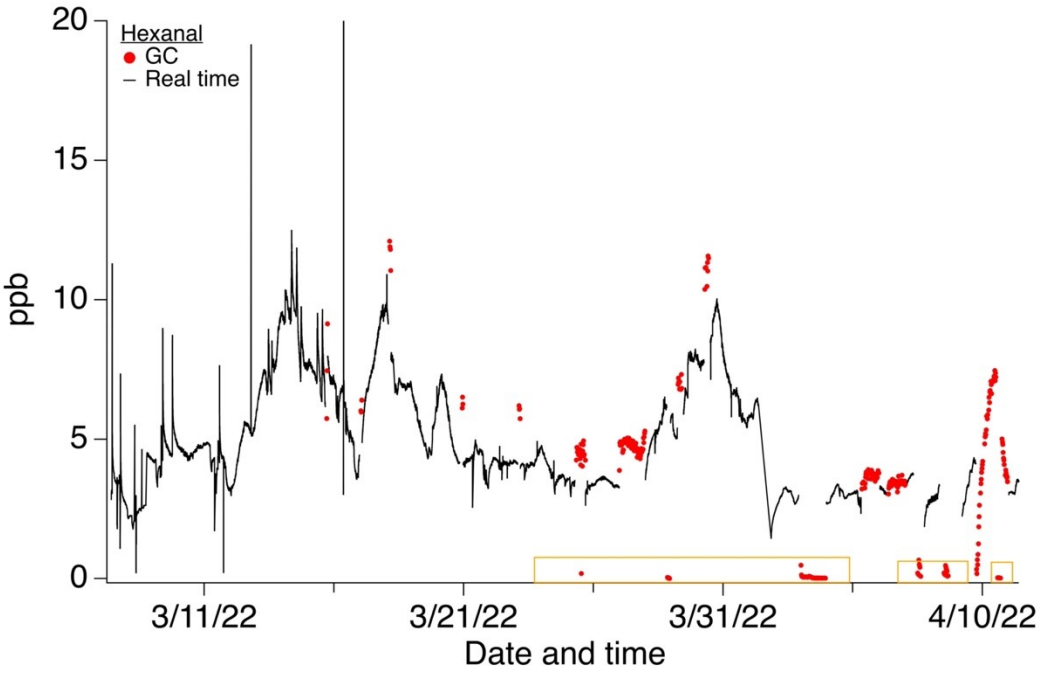

Figure S3. Comparison of real-time Vocus PTR-MS mixing ratio (black time series) and GC-PTR-MS mixing ratio (red markers) for hexanal throughout the campaign. Points in orange boxes represent outdoor GC samples. Data collected on 4/10/22 were collected as part of a temperature ramp in the house (Table S1).

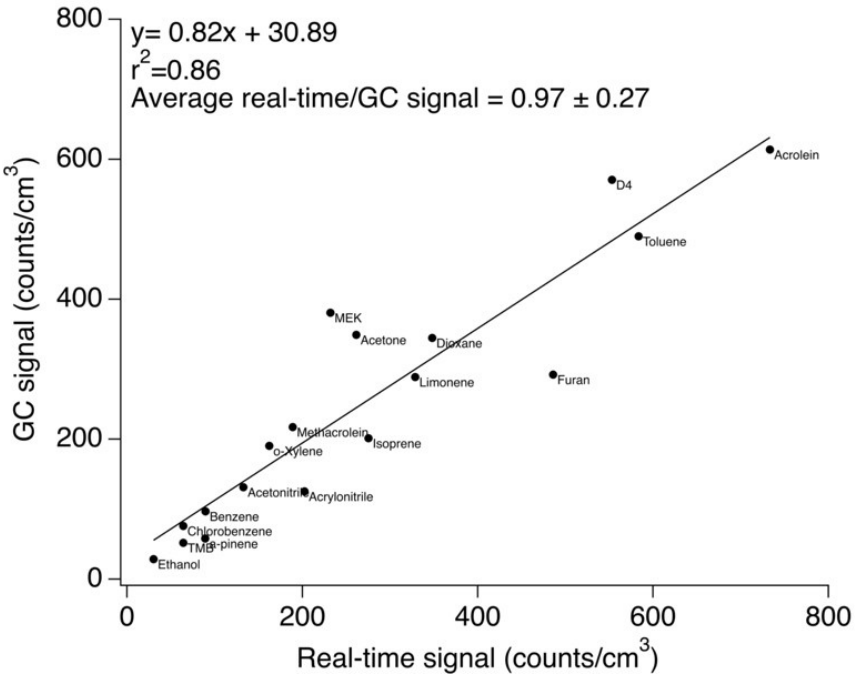

Figure S4. Comparison of real-time Vocus PTR-MS signal and GC-PTR-MS signal. The best fit line is also drawn on the plot; in general, there is agreement between the two measurements though some GC-PTR-MS signals are biased slightly low or high.

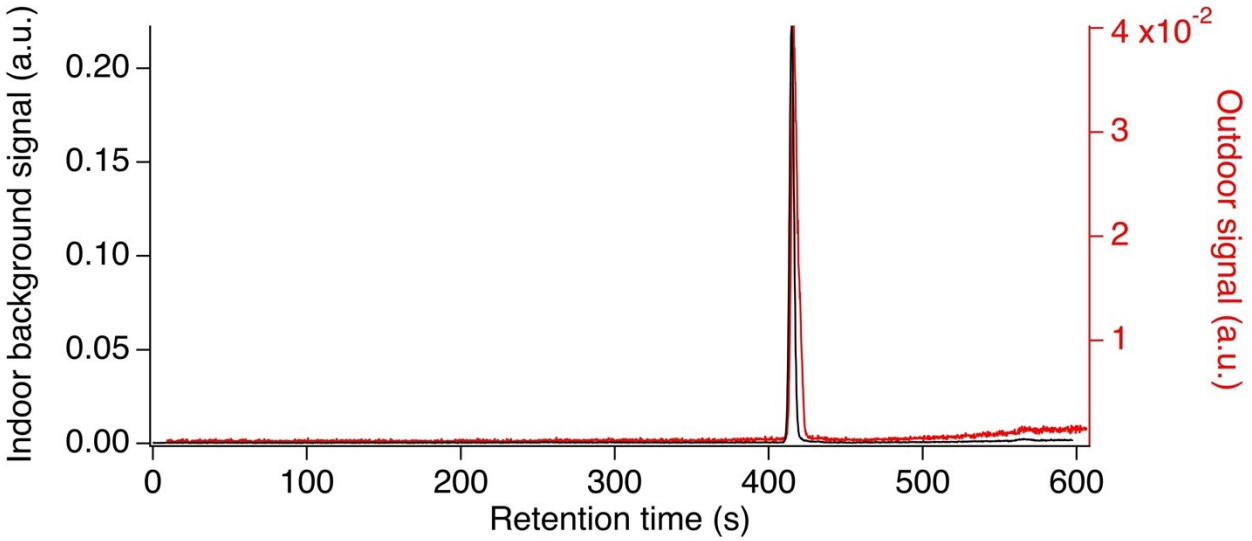

Figure S5. Extracted ion chromatogram for $C_8H_{24}O_4Si_4H^+$ (dominant peak corresponds to octamethylcyclotetrasiloxane, or D4 siloxane). The indoor y-axis (left hand side) is order of magnitude 10^{-1} while the outdoor y-axis (right hand side) is order of magnitude 10^{-2}.

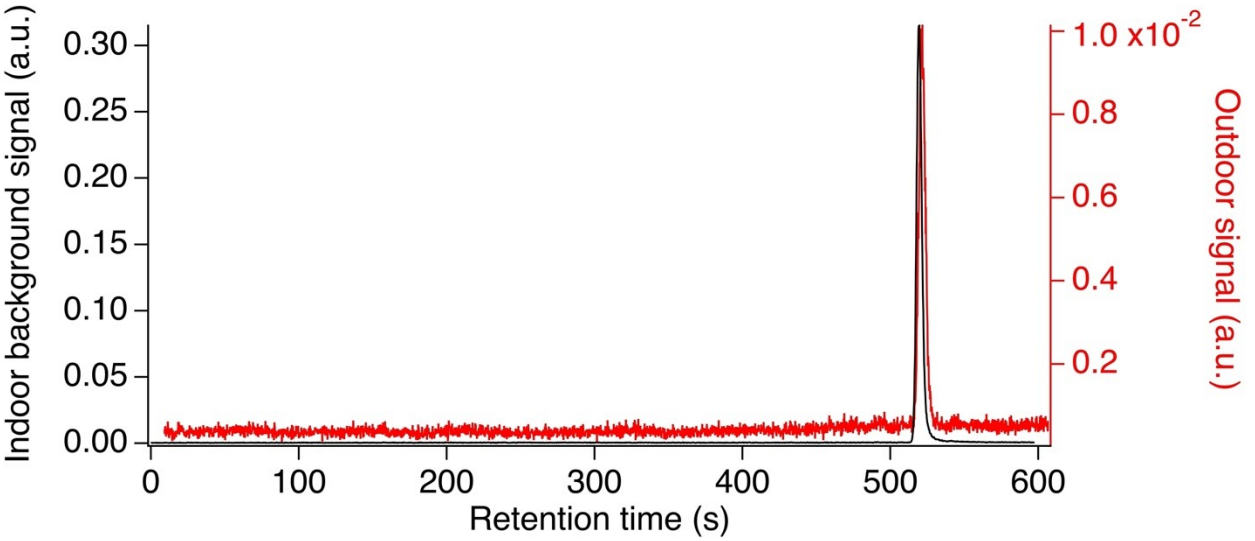

Figure S6. Extracted ion chromatogram for $C_{10}H_{30}O_5Si_5H^+$ (dominant peak corresponds to decamethylcyclopentasiloxane or D5 siloxane). The indoor y-axis (left hand side) is order of magnitude 10^{-1} while the outdoor y-axis (right hand side) is order of magnitude 10^{-2}.

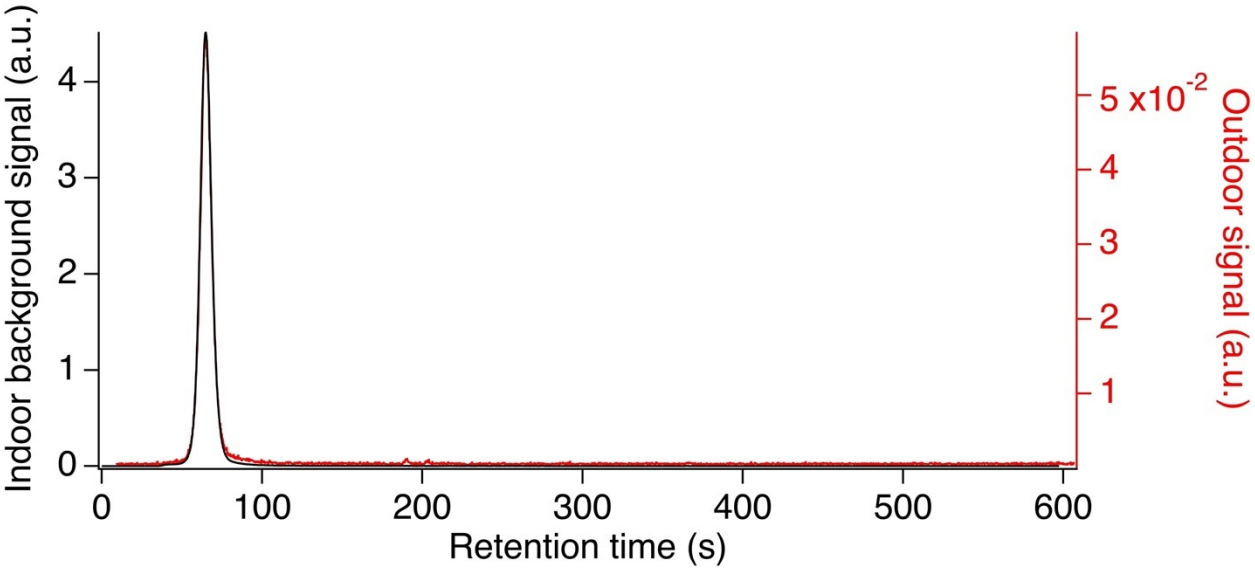

Figure S7. Extracted ion chromatogram for $C_2H_6OH^+$ (dominant peak corresponds to ethanol). The indoor y-axis (left hand side) is order of magnitude 10^0 while the outdoor y-axis (right hand side) is order of magnitude 10^{-2}.

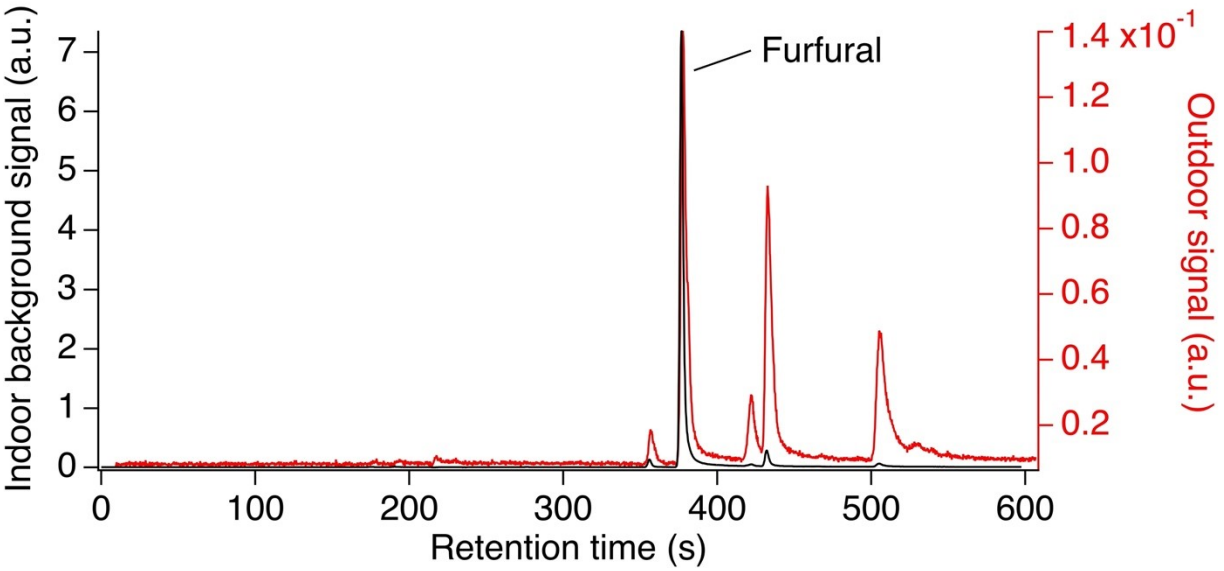

Figure S8. Extracted ion chromatogram for $C_5H_4O_2H^+$. The indoor y-axis (left hand side) is order of magnitude 10^0 while the outdoor y-axis (right hand side) is order of magnitude 10^{-1}.

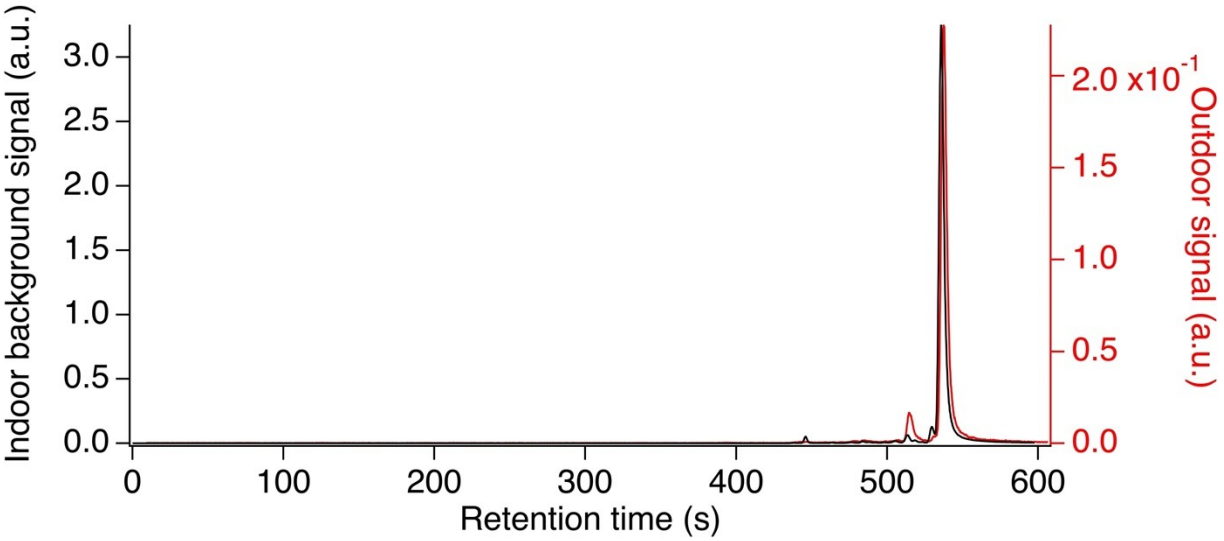

Figure S9. Extracted ion chromatogram for $C_9H_{18}OH^+$ (dominant peak corresponds to nonanal). The indoor y-axis (left hand side) is order of magnitude 10^0 while the outdoor y-axis (right hand side) is order of magnitude 10^{-1}.

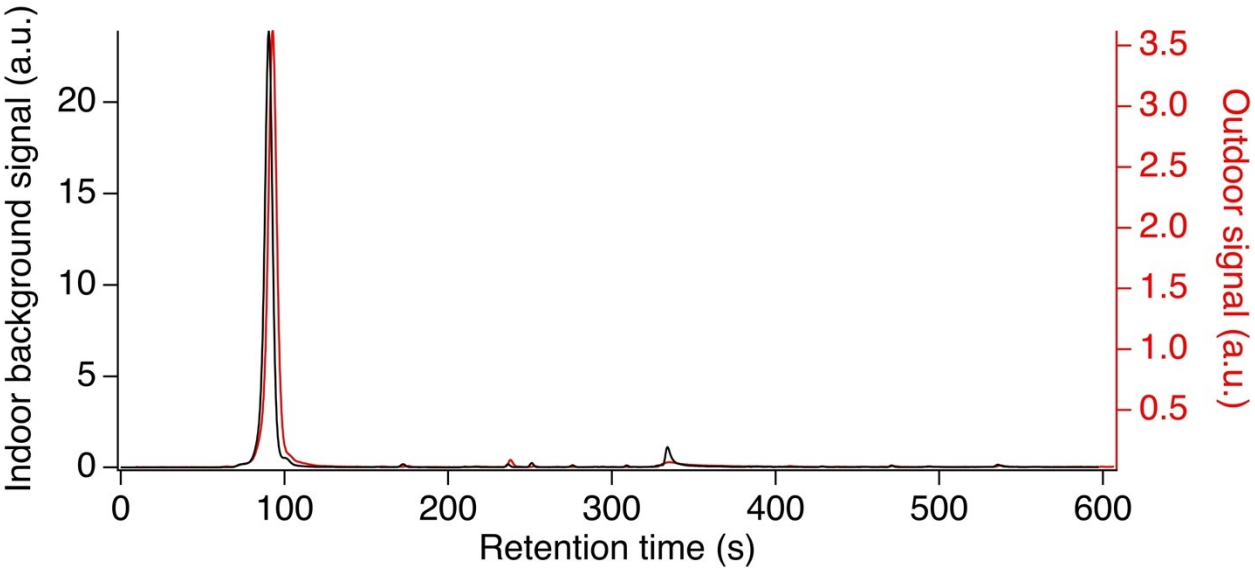

Figure S10. Extracted ion chromatogram for $C_3H_6OH^+$ (dominant peak corresponds to acetone). The indoor y-axis (left hand side) is order of magnitude 10^1 while the outdoor y-axis (right hand side) is order of magnitude 10^0.

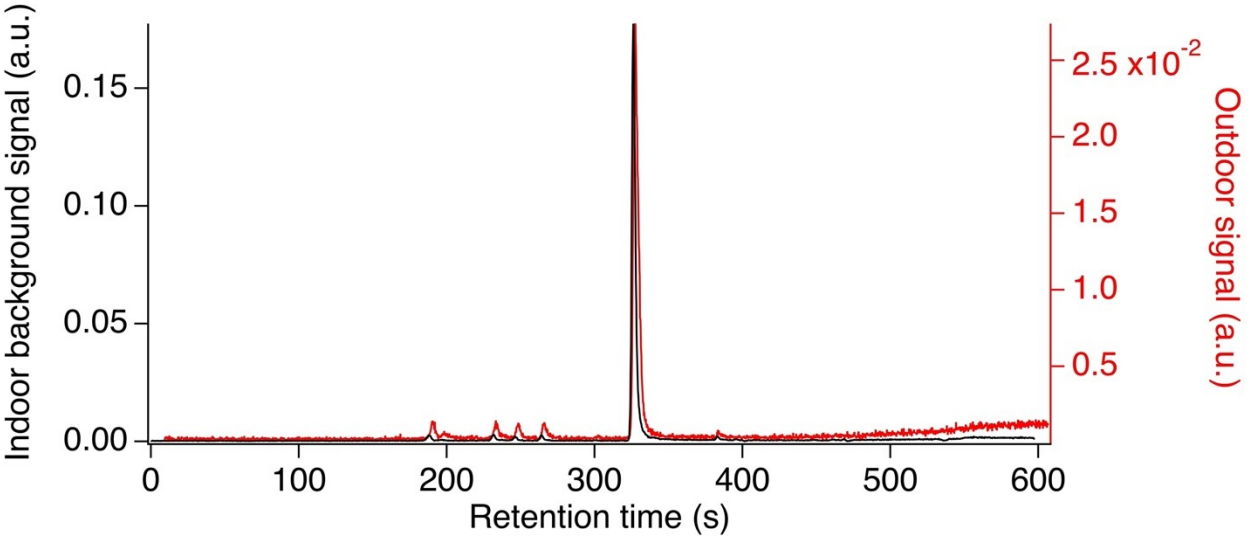

Figure S11. Extracted ion chromatogram for $C_4H_5NH^+$ (dominant peak corresponds to pyrrole). The indoor y-axis (left hand side) is order of magnitude 10^{-1} while the outdoor y-axis (right hand side) is order of magnitude 10^{-2}.

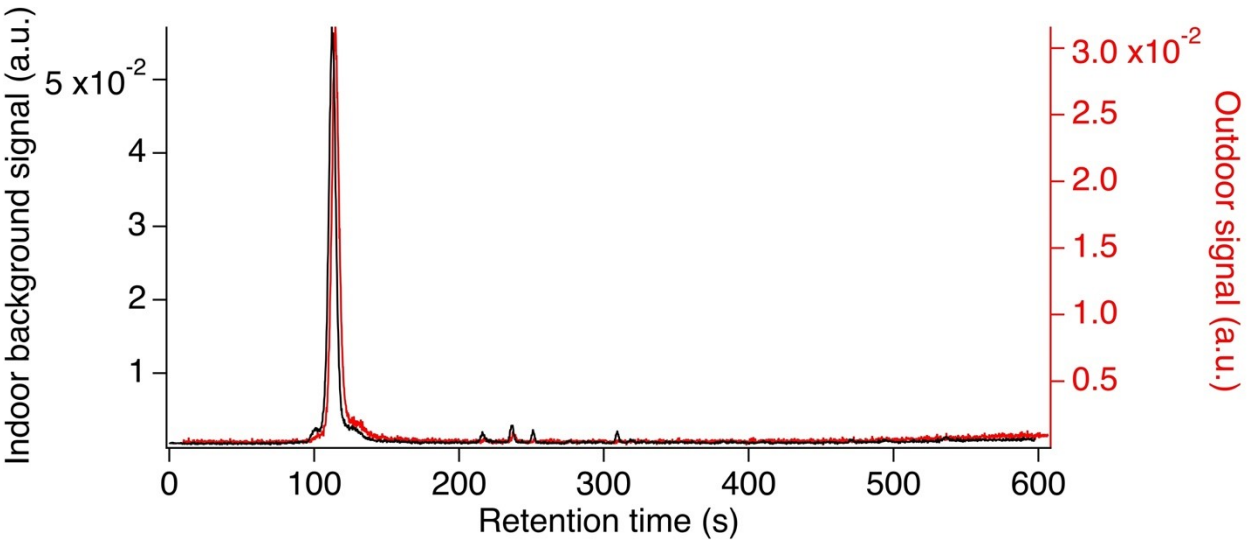

Figure S12. Extracted ion chromatogram for $C_2H_3NH^+$ (dominant peak corresponds to acetonitrile). The indoor y-axis (left hand side) is order of magnitude 10^{-2} and the outdoor y-axis (right hand side) is order of magnitude 10^{-2}.

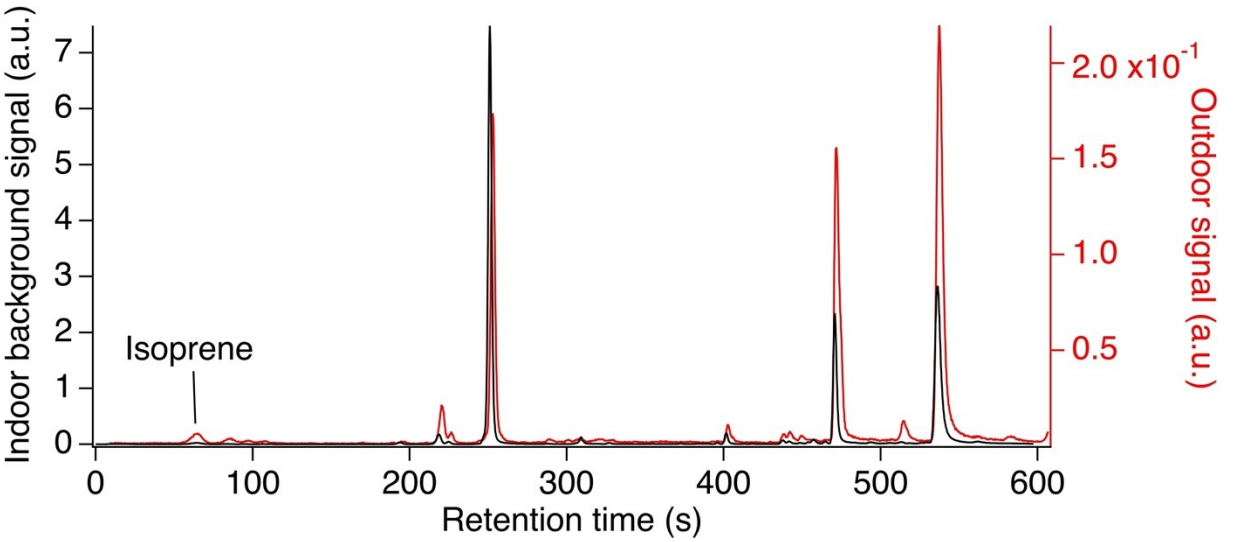

Figure S13. Extracted ion chromatogram for $C_5H_9^+$. The indoor y-axis (left hand side) is order of magnitude 10^0 while the outdoor y-axis (right hand side) is order of magnitude 10^{-1}.

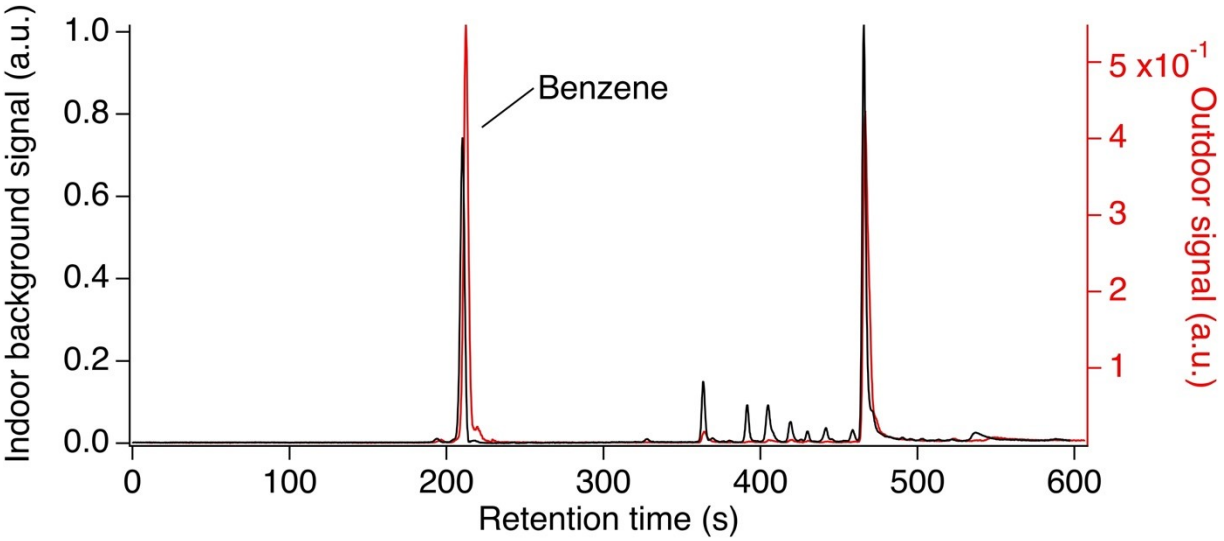

Figure S14. Extracted ion chromatogram for $C_6H_7^+$. The indoor y-axis (left hand side) is order of magnitude 10^0 while the outdoor y-axis (right hand side) is order of magnitude 10^{-1}.

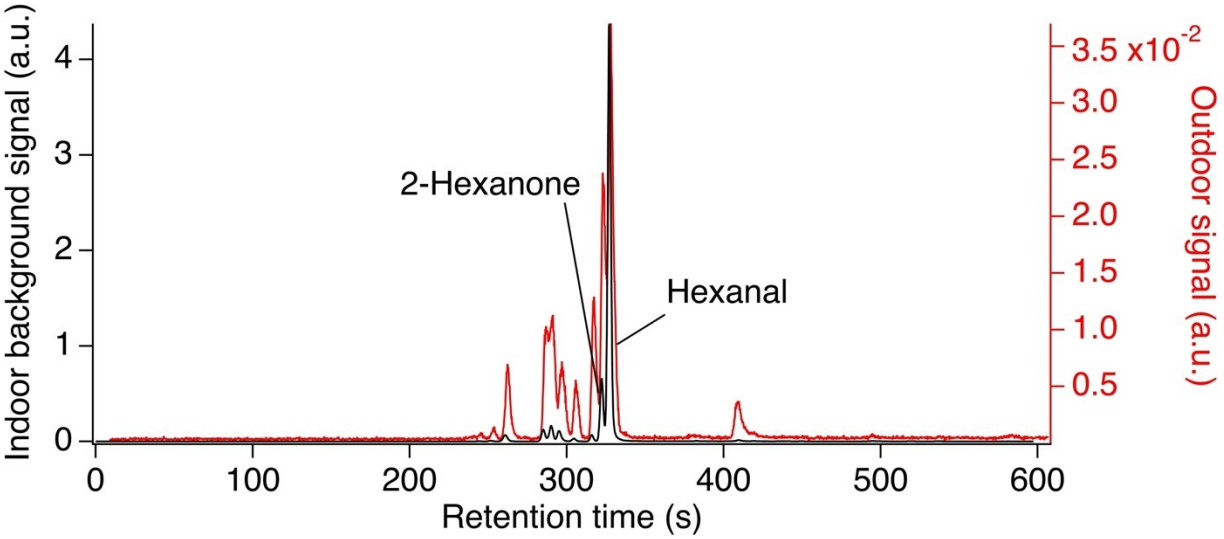

Figure S15. Extracted ion chromatogram for $C_6H_{12}OH^+$. The indoor y-axis (left hand side) is order of magnitude 10^0 while the outdoor y-axis (right hand side) is order of magnitude 10^{-2}.

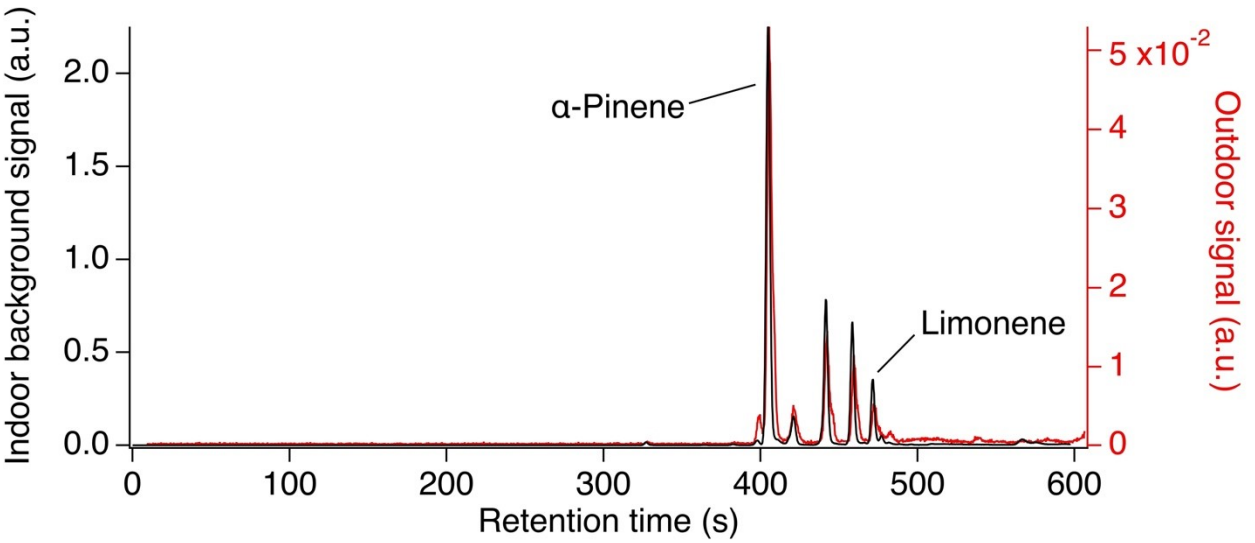

Figure S16. Extracted ion chromatogram for $C_{10}H_{17}^{+}$. The indoor y-axis (left hand side) is order of magnitude 10^{0} while the outdoor y-axis (right hand side) is order of magnitude 10^{-2}.

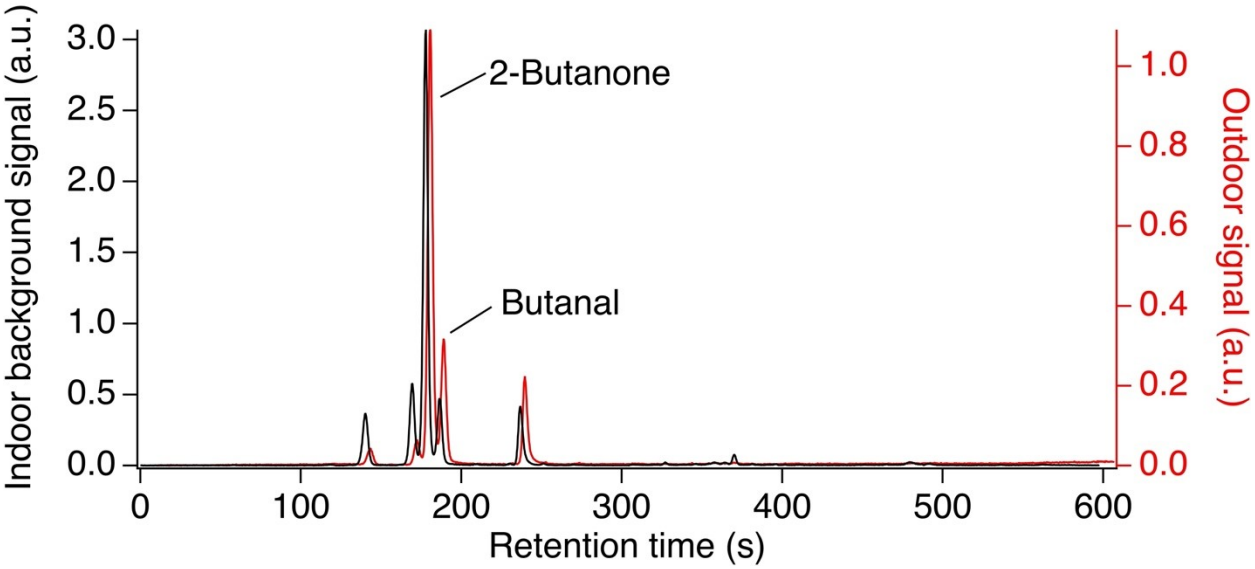

Figure S17. Extracted ion chromatogram for $C_4H_8OH^{+}$. The indoor y-axis (left hand side) is order of magnitude 10^{0} and the outdoor y-axis (right hand side) is order of magnitude 10^{0}.

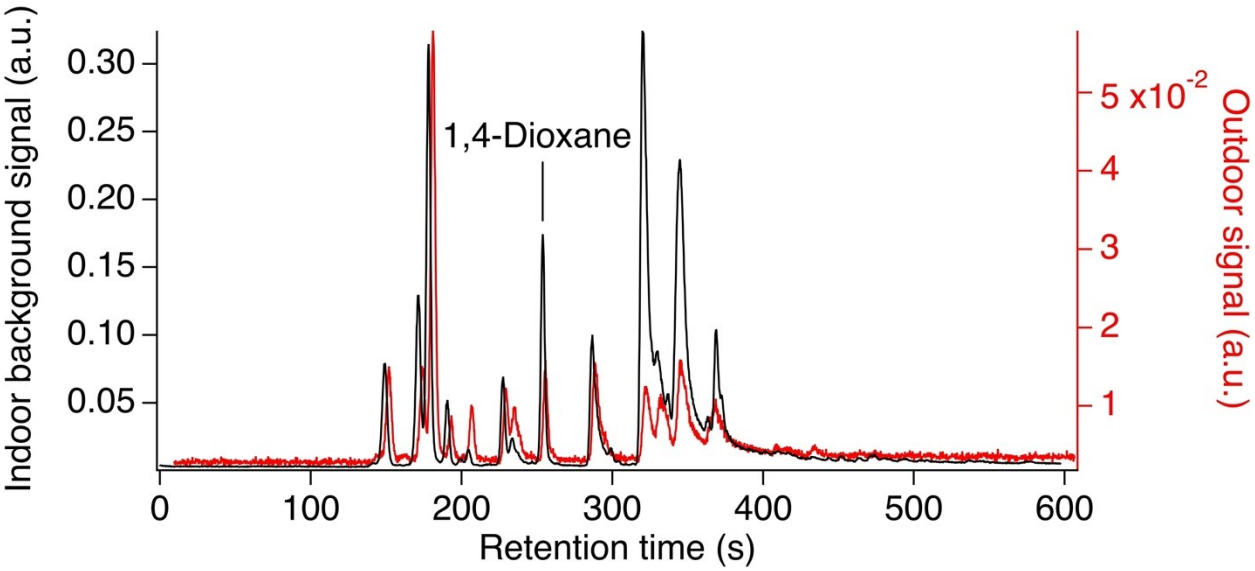

Figure S18. Extracted ion chromatogram for $C_4H_8O_2H^+$. The indoor y-axis (left hand side) is order of magnitude 10^{-1} while the outdoor y-axis (right hand side) is order of magnitude 10^{-2}.

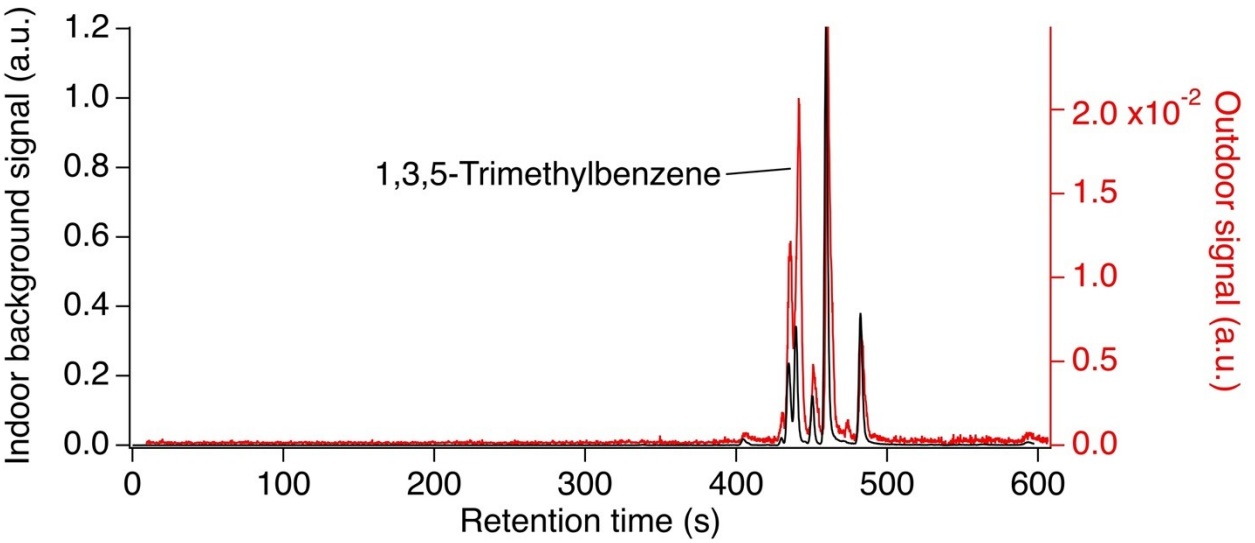

Figure S19. Extracted ion chromatogram for $C_9H_{13}^+$. The indoor y-axis (left hand side) is order of magnitude 10^0 while the outdoor y-axis (right hand side) is order of magnitude 10^{-2}.

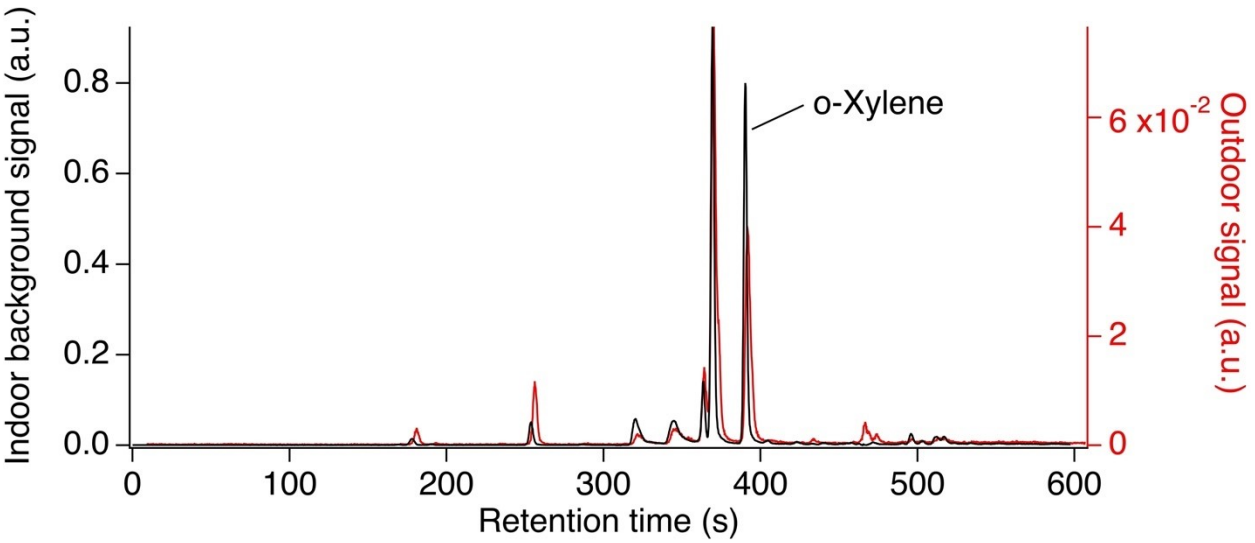

Figure S20. Extracted ion chromatogram for $C_8H_{11}^+$. The indoor y-axis (left hand side) is order of magnitude 10^{-1} while the outdoor y-axis (right hand side) is order of magnitude 10^{-2}.

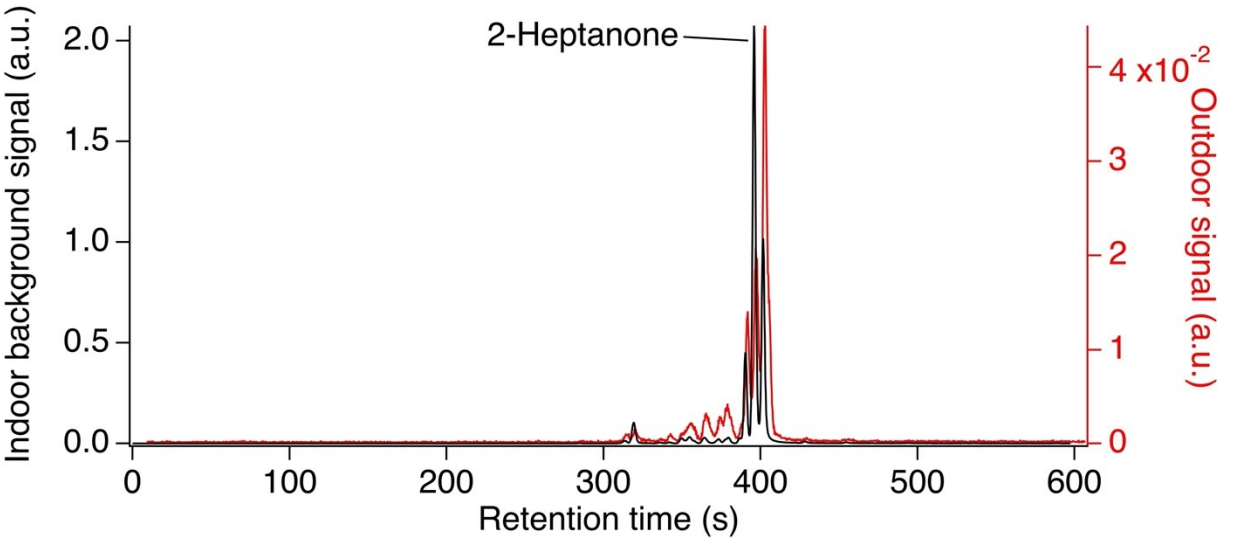

Figure S21. Extracted ion chromatogram for $C_7H_{14}OH^+$. The indoor y-axis (left hand side) is order of magnitude 10^0 while the outdoor y-axis (right hand side) is order of magnitude 10^{-2}.

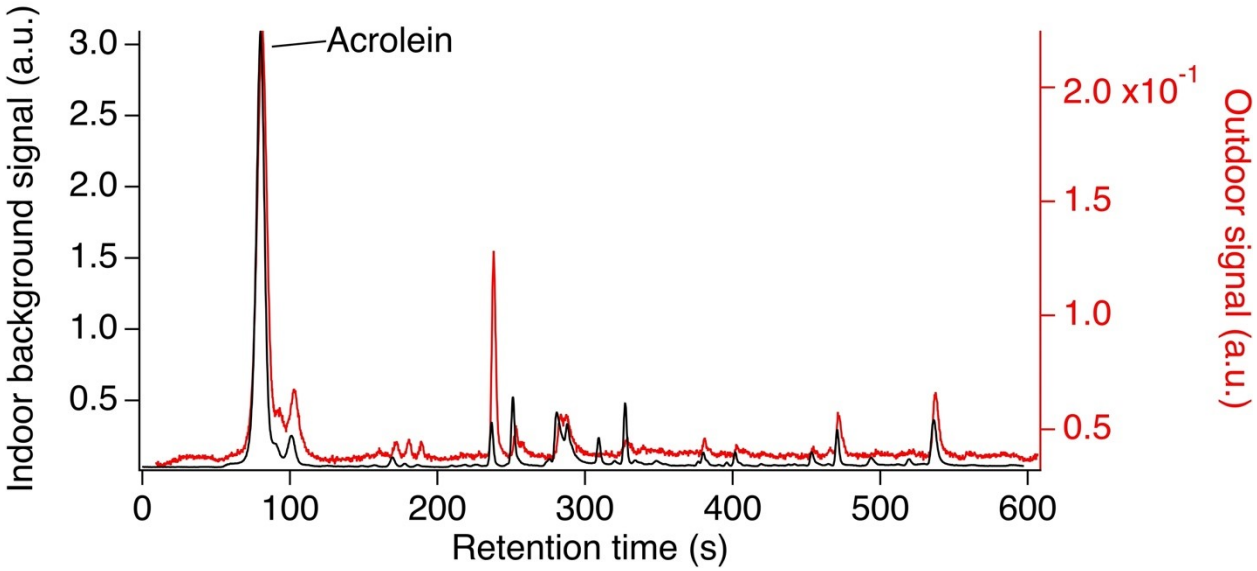

Figure S22. Extracted ion chromatogram for $C_3H_4OH^+$. The indoor y-axis (left hand side) is order of magnitude 10^0 while the outdoor y-axis (right hand side) is order of magnitude 10^{-1}.

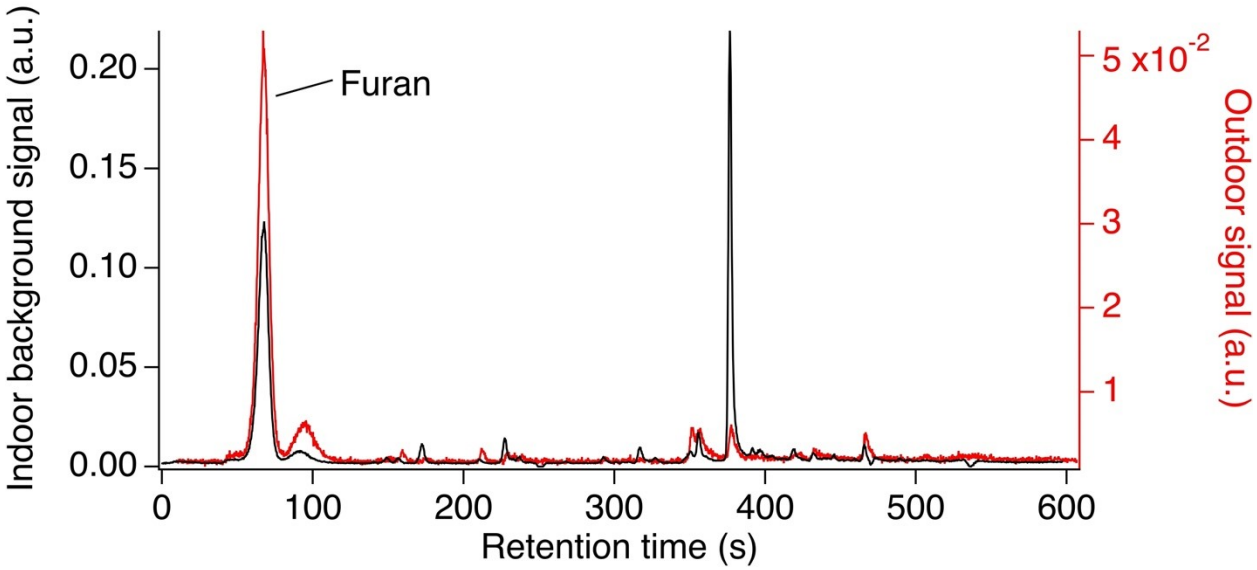

Figure S23. Extracted ion chromatogram for $C_4H_4OH^+$. The indoor y-axis (left hand side) is order of magnitude 10^{-1} while the outdoor y-axis (right hand side) is order of magnitude 10^{-2}.

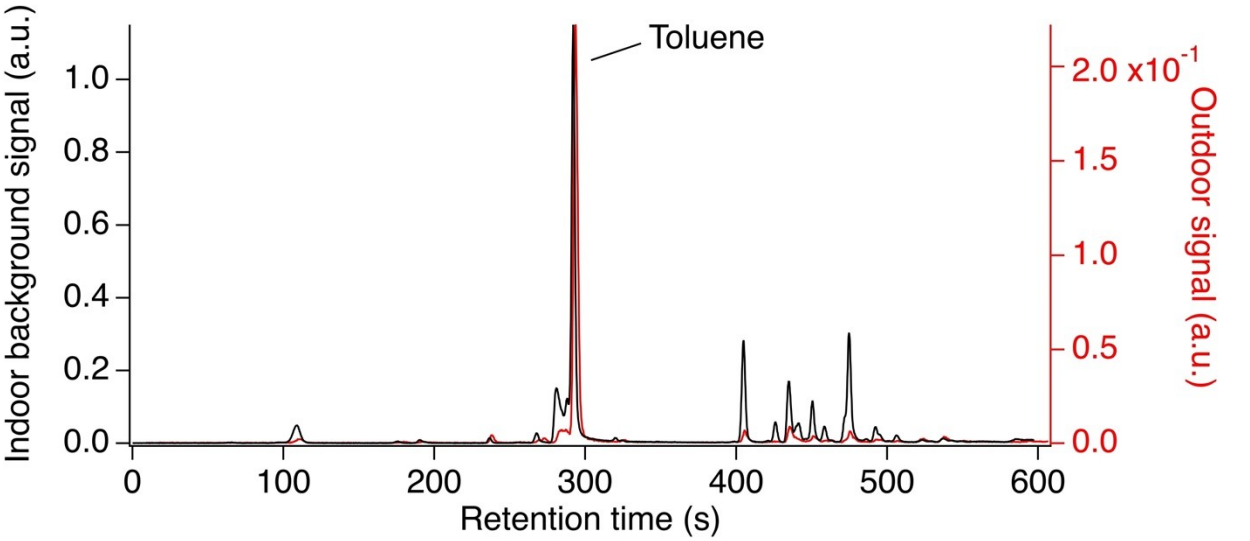

Figure S24. Extracted ion chromatogram for $C_7H_9^+$. The indoor y-axis (left hand side) is order of magnitude 10^0 while the outdoor y-axis (right hand side) is order of magnitude 10^{-1}.

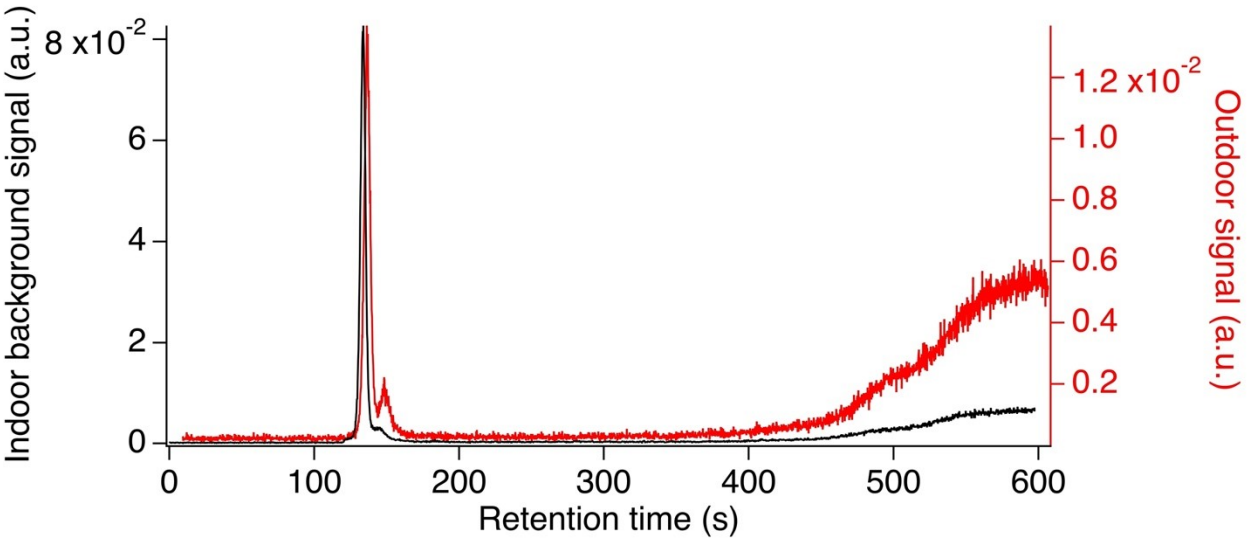

Figure S25. Extracted ion chromatogram for $C_3H_3NH^+$ (dominant peak corresponds to acrylonitrile). The indoor y-axis (left hand side) is order of magnitude 10^{-2} and the outdoor y-axis (right hand side) is order of magnitude 10^{-2}.

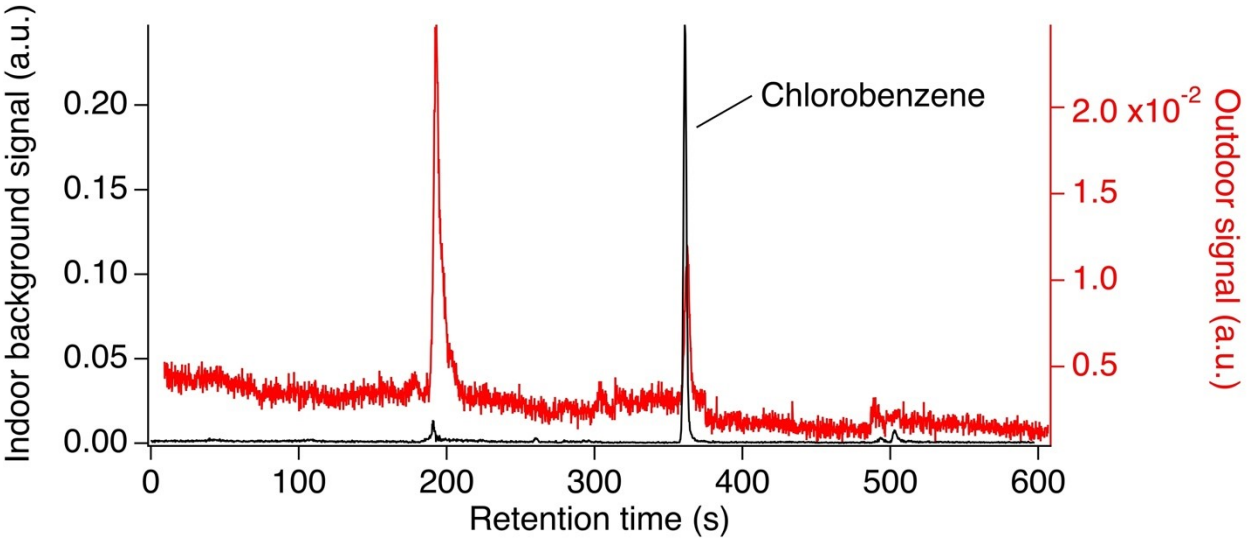

Figure S26. Extracted ion chromatogram for $C_6H_5ClH^+$. The indoor y-axis (left hand side) is order of magnitude 10^{-1} while the outdoor y-axis (right hand side) is order of magnitude 10^{-2}.

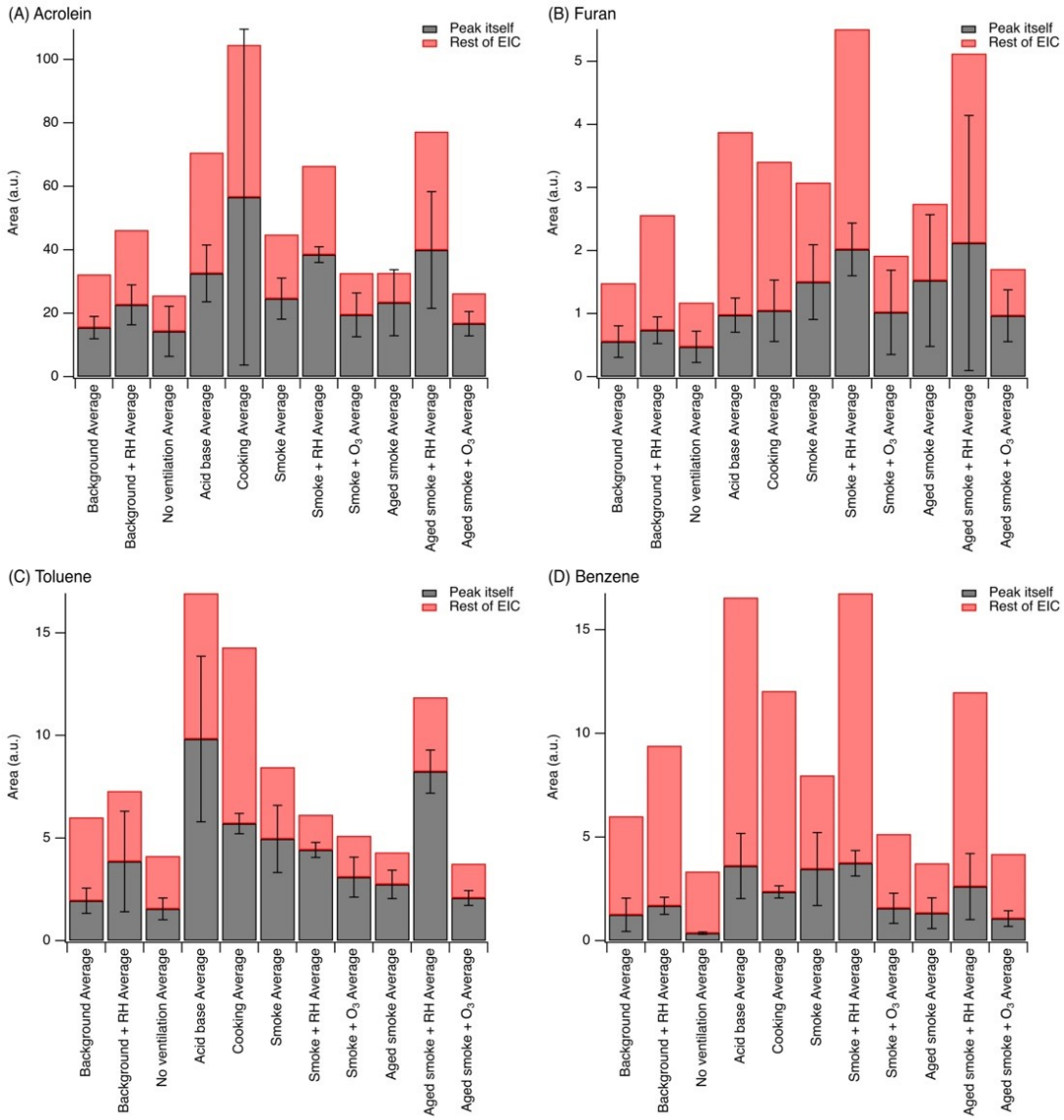

Figure S27. Comparison of changes in absolute peak area and absolute EIC area for select ions that showed increased sensitivity towards indoor environmental conditions.

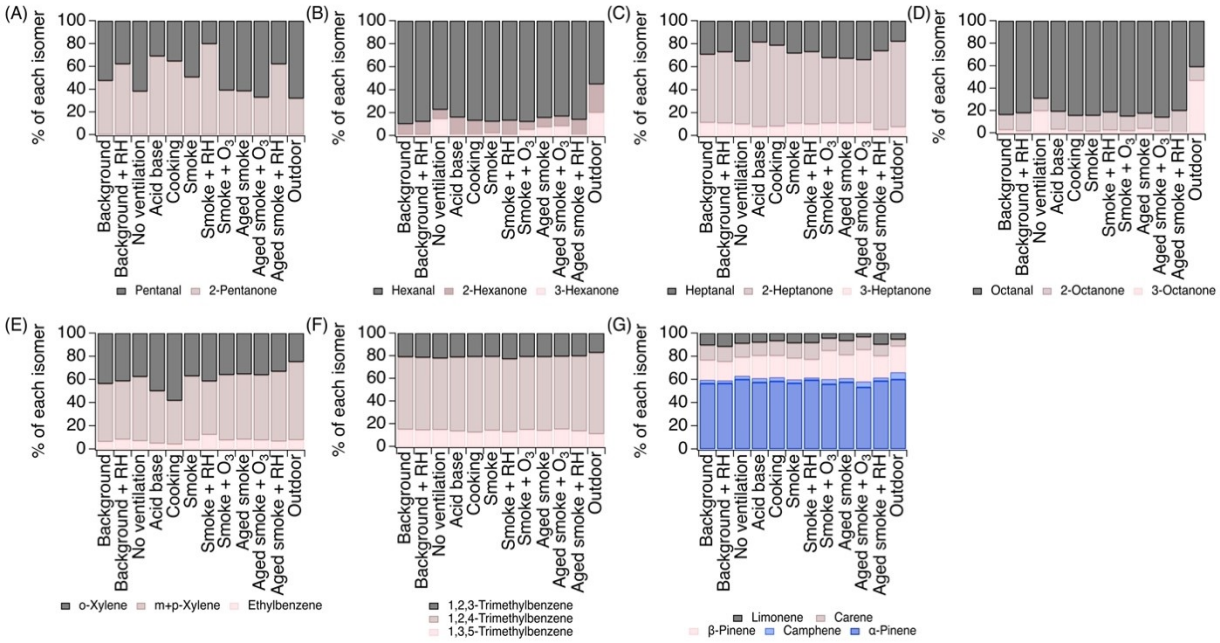

Figure S28. Isomer distribution for select species with consistently trackable isomers throughout the duration of the campaign. Individual isomer sensitivities are applied to each species. Data shown are for C5 carbonyls (A), C6 carbonyls (B), C7 carbonyls (C), C8 carbonyls (D), xylenes (E), trimethylbenzenes (F), and monoterpenes (G).

References

1. Coggon MM, Stockwell CE, Claflin MS, Pfannerstill EY, Lu X, Gilman JB, Marcantonio J, Cao C, Bates K, Gkatzelis GI, Lamplugh A, Katz EF, Arata C, Apel EC, Hornbrook RS, Piel F, Majluf F, Blake DR, Wisthaler A, Canagaratna M, Lerner BM, Goldstein AH, Mak JE, Warneke C. Identifying and correcting interferences to PTR-ToF-MS measurements of isoprene and other urban volatile organic compounds. 2023 Aug 28 [cited 2023 Dec 28]; Available from: https://egusphere.copernicus.org/preprints/2023/egusphere-2023-1497/

2. C. Heeley-Hill A, K. Grange S, W. Ward M, C. Lewis A, Owen N, Jordan C, Hodgson G, Adamson G. Frequency of use of household products containing VOCs and indoor atmospheric concentrations in homes. Environmental Science: Processes & Impacts. 2021;23(5):699–713.

3. Molinier B, Arata C, Katz EF, Lunderberg DM, Liu Y, Misztal PK, Nazaroff WW, Goldstein AH. Volatile Methyl Siloxanes and Other Organosilicon Compounds in Residential Air. Environ Sci Technol. 2022 Nov 15;56(22):15427–36.

4. Arata C, Misztal PK, Tian Y, Lunderberg DM, Kristensen K, Novoselac A, Vance ME, Farmer DK, Nazaroff WW, Goldstein AH. Volatile organic compound emissions during HOMEChem. Indoor Air. 2021;31(6):2099–117.

5. Wang C, Mattila JM, Farmer DK, Arata C, Goldstein AH, Abbatt JPD. Behavior of Isocyanic Acid and Other Nitrogen-Containing Volatile Organic Compounds in The Indoor Environment. Environ Sci Technol. 2022 Jun 21;56(12):7598–607.

6. Koss AR, Sekimoto K, Gilman JB, Selimovic V, Coggon MM, Zarzana KJ, Yuan B, Lerner BM, Brown SS, Jimenez JL, Krechmer J, Roberts JM, Warneke C, Yokelson RJ, de Gouw J. Non-methane organic gas emissions from biomass burning: identification, quantification, and emission factors from PTR-ToF during the FIREX 2016 laboratory experiment. Atmospheric Chemistry and Physics. 2018 Mar 7;18(5):3299–319.

7. Sleiman M, Logue JM, Luo W, Pankow JF, Gundel LA, Destaillats H. Inhalable Constituents of Thirdhand Tobacco Smoke: Chemical Characterization and Health Impact Considerations. Environ Sci Technol. 2014 Nov 18;48(22):13093–101.

8. Rösch C, Kohajda T, Röder S, Bergen M von, Schlink U. Relationship between sources and patterns of VOCs in indoor air. Atmospheric Pollution Research. 2014 Jan 1;5(1):129–37.

9. Ernle L, Ringsdorf MA, Williams J. Influence of ozone and humidity on PTR-MS and GC-MS VOC measurements with and without a $Na_2S_2O_3$ ozone scrubber. Atmospheric Measurement Techniques. 2023 Mar 7;16(5):1179–94.

10. Lee JH, Batterman SA, Jia C, Chernyak S. Ozone Artifacts and Carbonyl Measurements Using Tenax GR, Tenax TA, Carbopack B, and Carbopack X Adsorbents. Journal of the Air & Waste Management Association. 2006 Nov 1;56(11):1503–17.